Control of Thermal Power Plant Combustion Distribution Using Extremum Seeking

Aleksandra Marjanović, Miroslav Krstić, *Fellow, IEEE*, Željko Đurović, and Branko Kovačević, *Senior Member, IEEE*

***Abstract*— High demands for increasing robustness, safety, and efficiency in thermal power plants are the main motivation behind ongoing attempts to optimize combustion. This paper presents a study of modeling and control of the combustion process in a tangentially fired pulverized-coal boiler. It proposes an approach to flame geometry and position control by means of reallocation of firing. Such control ensures flame focus maintenance away from the walls of the boiler, and thus prevents many unwanted by-products of combustion. In addition, uniform heat dissipation over mills enhances the energy efficiency and reliability of the boiler. First, experimental data obtained from the 350-MW boiler of the Nikola Tesla power plant, Serbia, are analyzed in detail. This results in a model identification procedure using an adaptive parameter estimation method. Second, constrained multivariate extremum seeking (ES) is proposed in this paper, to optimally tune boiler operation in order to maintain the desired flame configuration in the furnace. Finally, the effectiveness of the ES adaptive controller in the presence of disturbances is demonstrated through simulations performed on the experimentally identified model of the boiler.**

***Index Terms*— Combustion distribution, disturbance rejection, extremum-seeking (ES) control, temperature distribution, thermal power plant.**

I. Introduction

COAL-THERMAL power plants account for the majority of power generation in the world. Energy efficiency and consumption are very important topics at present. The power generation market is focused on finding ways to enhance energy systems, in terms of reducing losses and maximizing availability and revenue. This paper considers temperature distribution regulation by reallocation of coal over mills as a way of overcoming many challenges of the combustion process. Due to constantly increasing demands of both consumers and the government, there are a number of papers dedicated to modeling and sophisticated control technologies of thermal power plant subsystems [1]–[4]. Given that combustion is one of the crucial processes, combustion control optimization is among the most important tasks. A proper control algorithm can significantly increase the efficiency of the process, which is one of the main goals in this type of systems. At the same time, the consequence of a poor control algorithm is low safety and reliability of the system. Namely, prolonged exposure to high temperatures inside the furnace shortens the lifetime of the components and can result in different types of failures. Over 30% of all boiler failures are caused by high temperatures. Whether the change is instant or gradual over time, high temperature can lead to unwanted deformations and material cracks. At the same time, the inevitable by-products of the combustion process are deposits of soot and slag on the walls of the boiler components. Soot and slag are products of molten ash, which is located on surfaces that absorb heat by emission. Large amounts of soot and slag in the bottom section of the boiler contribute to higher temperatures and deposits in the top section of the boiler. These deposits decrease the heat transfer, along with the coefficient of efficiency [5]. Therefore, it is necessary to maintain the temperature inside the boiler below the melting point of the ash, so that it can be disposed of using the ash transport system. Additional harmful products of combustion are oxides of nitrite, sulfur, and carbon. Environmentalists are continually increasing their demands when it comes to emissions of these oxides. Some of the potential solutions involve fuel additives, alternative fuels, and low NOx burners. Others employ more intelligent and complex control algorithms.

In general, insufficient monitoring and inadequate control are usually followed by boiler operation under the recommendation of the manufacturer or experienced operators. Over the past decades, many different approaches have been designed to enable better monitoring and understanding of the combustion process. From a theoretical point of view, expert knowledge was shaped into computational fluid dynamics (CFD), as a tool for analyzing the influence of different fuels, geometry, and firing onto the combustion process [6]–[9]. Although CFD is very useful for simulating different phenomena, it employs large amounts of data and is, therefore, not convenient for online procedures. In other words, CFD provides extensive understanding of the process, but it is not too useful when it comes to real-time use. As a response to this kind of theoretical

Manuscript received October 16, 2015; revised July 18, 2016; accepted November 2, 2016. Date of publication November 29, 2016; date of current version August 7, 2017. Manuscript received in final form November 7, 2016. This work was supported by the Ministry of Education and Science of the Republic of Serbia, research projects under Grant TR32038 and Grant III42007. Recommended by Associate Editor A. Serrani.

A. Marjanović, Ž. Đurović, and B. Kovačević are with the Department of Signals and Systems, School of Electrical Engineering, University of Belgrade, 11120 Belgrade, Serbia (e-mail: amarjanovic@etf.bg.ac.rs; zdjurovic@etf.bg.ac.rs; kovacevic_b@etf.bg.ac.rs).

M. Krstić is with the Department of Mechanical and Aerospace Engineering, University of California at San Diego, San Diego, CA 92093 USA (e-mail: krstic@ucsd.edu).

Color versions of one or more of the figures in this paper are available online at http://ieeexplore.ieee.org.

Digital Object Identifier 10.1109/TCST.2016.2627499

initiative in terms of a complex and informative simulator, many companies have made significant efforts to provide appropriate sensors that would enable better monitoring of the combustion process. For instance, modern sensor systems (e.g., pyrometers) offer the possibility of visualizing the combustion process using a 3-D temperature distribution [10]. They are used by the operator to perceive the behavior of the system, but at the same time, they can be used for control system enhancement. There are many papers that deal with combustion process optimization. Some of them use the aforementioned CFD in order to reduce the amount of ash in the burning process [11]. Others combine genetic algorithms with neural networks to achieve the highest boiler heat efficiency based on modeling of the carbon burnout [12] or, with support vector machines, to lower the NOx emission in selective catalyst reaction equipped systems [13]. Novel approaches combine parallel-type and cross-limiting-type techniques to overcome the limitations of both [14]. Nevertheless, many papers focus on only some of the problems. A more complex approach is to adjust control signals so as to influence the flame geometry, maintaining it as centralized and as symmetric as possible. This would help overcome all the mentioned challenges of the combustion process. However, controlling temperature distribution is not an easy task. Since the physics of the process is very complex, different modern optimization tools have been tested in solving these requirements. Some attempts have been made to approach this problem using information about the bias of the flame from the center of the furnace, as described in [15]. On the other hand, [16] presents temperature distribution control using density function shaping based on B-spline expansion and model predictive control. In general, there are two main approaches. One relies on detailed modeling of the process physics. As such, it is very complex and not suitable for online application. The other focuses on defining an appropriate model-free criterion and a tool for its optimization.

We suggest the use of the extremum-seeking (ES) algorithm as an optimization tool. Although the basics of ES were set in the early 1920s, it was not until the end of 20th century that it secured an important role in both theory [17]–[19] and practice [20]–[23]. The aim of the Extremum seeking control (ESC) is to design a control algorithm that drives the parameters of the system toward their optimal value. For some systems, the question of optimality is easily formulated, such as minimizing the net power output [24]. For others, an objective function is a result of thorough analysis of system behavior and can be defined using available measurements. In either case, the model of the system is not needed in the optimization process, which is usually highlighted as an advantage of this approach. On the other hand, the cost function can include model and other dynamic related parameters of the system [25]. The main drawback of this approach is its sensitivity to model uncertainties. A widely known application of ESC is optimization of the step response of combustion timing for Homogeneous charge compression ignition engines [26], antilock braking systems design [27], increasing the efficiency in photovoltaic systems [28], and so on. ES was proved successful in the optimization of thermal power plant boiler operation, in terms of minimizing NOx production [29]. In the absence of disturbances, ES performs model-free online updates of controller parameters and asymptotically achieves optimal steady-state performance. Since ES achieves exponential stability of a periodic solution that is $O(1/\omega)$-close to the optimal steady state, this exponential stability property also achieves appropriate local robustness to disturbances (based on a converse Lyapunov theorem and a standard robustness argument for vanishing or nonvanishing perturbations), as long as the disturbances are "uncorrelated" with the perturbation signals in the ES algorithm (over either the finite period of the ES perturbation or over the infinite time interval). If the disturbance is stochastic whereas the ES perturbation signals are deterministic, the analysis is less straightforward as neither deterministic nor stochastic averaging alone can be applied. A result of this nature was developed by Stankovic *et al.* [30]. There are also several applications of ES with disturbance rejection. Satisfying ESC performance for a single mode-locked laser under the influence of significant changes in the birefringence is presented in [31]. Article [32] analyzes the behavior of a variable-gain controller for motion control of a wafer scanner in the presence of unknown periodic disturbances. However, a rigorous proof of ESC convergence in the presence of disturbances imposes strict limitations. A robust design of a numerical optimization-based ES algorithm is presented in [33]. Reference [34] discusses the assumptions under which ES guarantees convergence of a periodic steady state using the concept of semiglobal asymptotic stability. Reference [35] considers tracking ES controllers with an adaptive control magnitude level sufficient for the suppression of disturbances and uncertainties. A comparison of different ES approaches and their convergence in application to energy efficiency of a vapor compression system is provided in [36].

This paper presents an approach to modeling and control of the combustion process in terms of regulating spatial temperature distribution. First, a cross-correlation analysis of measurement signals relevant to the combustion process was performed. This offered better understanding of the influence of firing on flame behavior, enabling a simpler model of the system with doser speeds as inputs and temperature measurements as outputs. Parameter estimation and model testing were performed on real measurements obtained at the thermal power plant Nikola Tesla, Obrenovac, Serbia. Second, analysis of real process measurements enabled an adequate control algorithm setup in terms of formulating the objective function. One of the main contributions of the paper is the aforementioned cost function, which is carefully defined using only real temperature measurements of the process, as a measure of symmetry of the flame geometry. The ES approach was used as a mechanism for the minimization of such function. It provided optimal doser speeds and thus optimal coal allocation per mill. The proposed algorithm was tested in simulations on the experimentally obtained model in the nominal state and in the presence of a simulated disturbance. It showed significant and promising results in both cases.

This paper is organized as follows. Section II provides a description of the combustion process and available sensor system. Section III considers detailed process

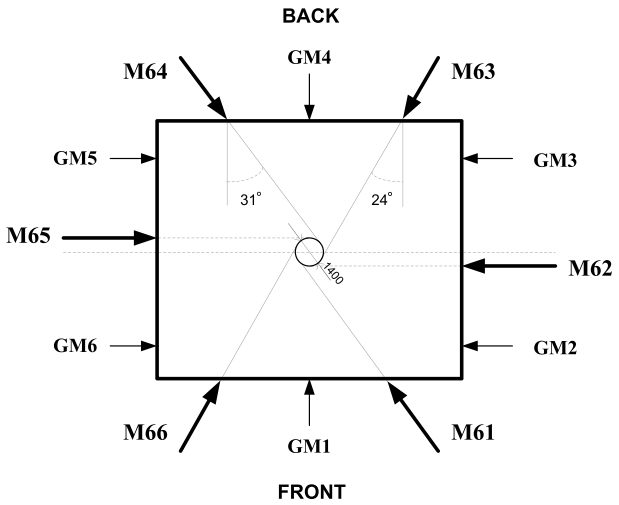

Fig. 1. Displacement of mills (M61–M66) and oil fuel burners (GM1–GM6) in block A6 of thermal power plant Nikola Tesla, Obrenovac, Serbia.

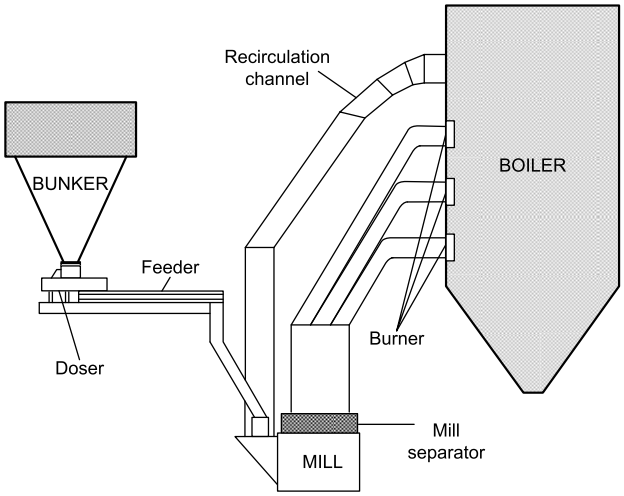

Fig. 2. Structure of the firing process. Coal transportation from the bunker to the boiler.

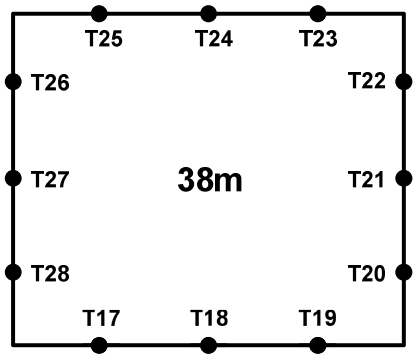

Fig. 3. Configuration of the pyrometer sensor system at 38 m of height: three per side of the boiler.

analysis using the cross-correlation functions of different relevant measurement signals. Also, it presents an identification procedure of a combustion model based on a weighted recursive least square (WRLS) algorithm. This model is further used in simulations concerning the analysis of the proposed control algorithm in Section IV. Prior to employing the gradient ESC algorithm, Section IV introduces a flame geometry-based cost function, considering certain control constraints. The implementation of the proposed control approach and relevant results are presented in Section V. The conclusions are stated in Section VI.

II. Combustion Process Description

The thermal power plant Nikola Tesla A (TENT A) is located in Obrenovac, Serbia. It consists of six units with an overall nominal power of 1650 MW. Lignite coal with a low and variable calorific value (5000–9000 kJ/kg) is used as a regular fuel in all six blocks. Auxiliary oil fuel is used in the firing process and for supporting fire with low calorific value coal firing. The unwanted by-products of the firing process are large amounts of ash and slag, as well as the oxides of carbon and nitrite, which increase environmental pollution.

This paper focuses on the combustion process in unit A6, whose nominal power is 350 MW. The main control task is to maintain the reference block power, while also controlling the fresh steam pressure in front of the turbine. One way to achieve this is to control the amount of coal and fresh air inserted into the boiler. Fig. 1 shows the A6 unit with six mills. The required amount of coal is, therefore, divided onto six parts, giving the operators a certain degree of freedom during partitioning. The mills are positioned so as to form a tangential configuration of the furnace. Fig. 1 also shows the displacement of the six oil fuel burners used to support fire during ignition and some unexpected events.

Combustion air is introduced by means of a fresh air fan and is used in several stages of the process. Lignite coal is transported from a bunker, using dosers and mill feeders. The amount of transported coal is proportional to the doser speed. The coal is fed to the mill after partial drying in a recirculation channel. Final coal drying, together with the pulverization process, takes place inside the mill. The so-called air mixture is forwarded to the mill separator. There, under the influence of inertia, insufficiently pulverized particles are extracted and returned back to the mill for repulverizing. The aero-mixture consisting of dried coal and transport medium is transported from the mill separator through the channels to the burners. Fig. 2 shows the described coal grinding process.

During reconstruction of the unit A6, a distributed control system was introduced, which provided additional possibilities in terms of control process quality. An SCADA system and a novel sensor system consisting of 42 pyrometers and several thermographic cameras are used for data monitoring and storage. The pyrometers are distributed over five different levels (heights) of the boiler. Depending on the physical condition of the furnace and the experience of specialists, the number of pyrometers varies with height. The levels at 17 and 51 m are equipped with 4 pyrometer units per level, while there are 12 pyrometers per level at 25, 38, and 43 m of height (Fig. 3). The pyrometers are two-color processing units, meaning that

the measurements are obtained at two close wavelength ranges (0.96 and 1.05 μm). The Plank radiation law provides the information about two significant values: one-color and two-color temperature. Due to the measuring method, the value of the two-color temperature is under a weak influence of half transparent obstacles in the optical path, such as smoke, steam, and unburned coal particles. Thus, it approximately corresponds to the maximum temperature of the optical path. On the other hand, the one-color temperature is under the influence of the aforementioned obstacles and represents the effective temperature of the optical path. Therefore, the difference between these two temperature estimations is a measure of combustion process efficiency.

This kind of sensor system structure enables detailed monitoring of temperature and its distribution within the boiler. It provides sufficient data for the identification procedure presented in Section III, which will contribute to the understanding of system behavior and the proposal of the adequate control algorithm. Note that there are high intensity disturbances inside the boiler caused by a change in coal quality, grinding, and the like. These disturbances are directly mapped on the fire forming and temperature distribution inside the boiler, which additionally complicates the identification procedure.

III. Combustion Process Identification

Combustion is a very complex process and the boiler is a highly distributed system. Therefore, the number of parameters needed for an adequate model of the system was expected to be high. The measurements were obtained from SCADA and pyrometer sensor systems. The output control signal of the main firing regulator refers to the overall amount of fuel. Within the DCS system, the operator has the possibility of adjusting mill loads according to their own knowledge and experience. Depending on the values set by the operators, the reallocation includes all the mills active in the automatic mode. Different experiments were carefully designed in order to support testing of the influence of firing distribution on spatial temperature distribution. Temperature analysis within one cross section gave insight into the flame position within that section. Practice dictated a central position of the flame, in order to avoid nonuniform loading of the pipe system, flame and combustion asymmetry, and so on. All the experiments were conducted and stored under regular conditions at a nominal load of 348 MW. A persistent reference signal was used to identify individual influences and input–output dependences, in order to obtain meaningful results. Figs. 4 and 5 show the measurements that correspond to the experiments. Fig. 4 shows dictated mill feeder speeds in both manual (constant speed values in long time intervals) and automatic modes. This section proposes a system identification method that focuses on the spatial temperature distribution as an output and mill loads as inputs of the system. The resulting model is later used to verify the proposed control algorithm.

A. System Cross-Correlation Analysis

In order to fully comprehend the nature of the process, we suggest a cross-correlation analysis as an introduction to

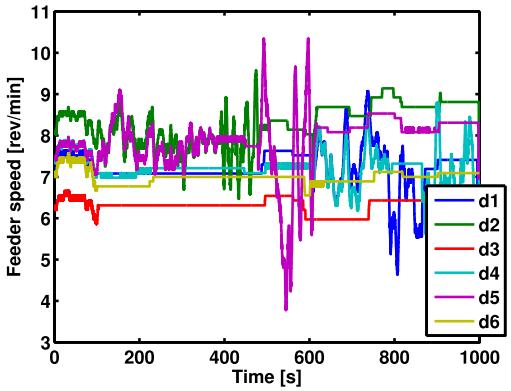

Fig. 4. Mill feeder speeds, proportional to mill loads.

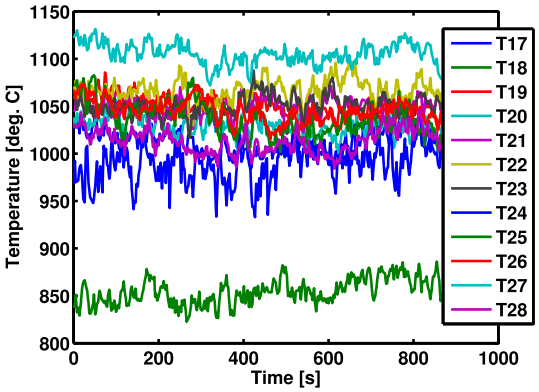

Fig. 5. Temperature measurements at 38 m of height.

the model identification procedure. The goal is to recognize the relation of the reallocation of overall load to the specific mill circles and the spatial temperature distribution in the furnace. As mentioned before, the system is under the constant influence of disturbances. As a way of suppressing these unwanted phenomena in terms of meaningful cross-correlation results, we propose subtraction of appropriate temperatures. Consider the described system with individual mill loads as inputs and differences in pyrometer temperatures as outputs. Using cross-correlation functions of individual input–output pairs, it is possible to determine how each input affects each output. The unbiased estimation of the cross-correlation function between input signal $d_i(m)$ and output signal $dT(m)$ is given as

$$r(m) = \frac{1}{N-m} \sum_{k=1}^{N-m} d_i(k) dT(k+m) \tag{1}$$

where N represents the length of the windowed sequences. As a result, the cross-correlation function value will be high for highly correlated signals and around zero for those input–output pairs that are not correlated.

More meaningful results can be obtained by analyzing the impact of different mills on the temperature differences on each side of the boiler, instead of the temperatures themselves. Let us examine the influence of simultaneous load/relief of

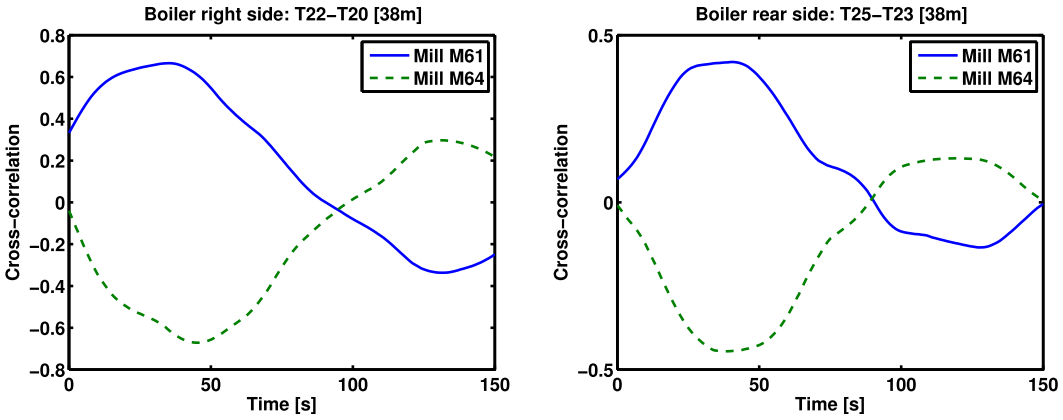

(a) (b)

Fig. 6. Influence of simultaneous load/relief of mills 1 and 4 on temperature difference in (a) right-hand side area of the boiler and (b) rear area of the boiler.

mills M61 and M64 on the temperature distribution at the height of 38 m (Fig. 6). The solid blue line in Fig. 6(a) experiences a peak at around 40 s, suggesting that the doser speed of M61 is positively correlated with the temperature difference $T_{22} - T_{20}$, suggesting greater positive influence of mill M61 on temperature T_{22} than temperature T_{20}. This means that the flame center shifts toward the rear side of the boiler as the load of mill M61 increased. On the other hand, the broken green line shows the opposite impact of mill M64. This result was expected bearing in mind the fact that the mills are positioned diagonally with respect to the furnace center. Similar conclusions can be drawn from Fig. 6(b). It illustrates the maximum, positive correlation between the difference of temperatures on the rear side of the furnace $T_{25} - T_{23}$ and mill M61 load. The same temperature difference was negatively correlated with the speed of M64 doser, meaning that the flame moved left as the M64 load decreased or right as it increased. In other words, the flame shift could be forced in the desired direction by reallocation within a certain pair of feeders. In this paper, we provide only the results of the cross-correlation analysis for mills M61 and M64, but similar conclusions could be made for the other two pairs of mills (M62–M65 and M63–M66). Also, Fig. 6 shows peaks in correlation around 40–50 s, suggesting the greatest influence of mills after that period of time, which was supported by the operators' experience. An additional cross-correlation analysis showed a similar mill influence at different heights, so a detailed presentation of those results is omitted from this paper. Again, this was consistent with the empirical findings of the experienced power plant engineers. These conclusions are important as they allowed for certain simplifications of the identification procedure and the control algorithm itself.

B. Parameter Estimation Algorithm

The main purpose of the cross-correlation analysis was to provide insight into the most important relations between system inputs and outputs, in order to support some model simplifications. Section III-A provided only the most important results of the cross-correlation analysis. The general conclusion was that the influence of the doser speed (proportional to the mill load) on temperatures is significant and similar at medium levels (at 23, 38, and 43 m) and less so at the bottom and top levels (17 and 51 m) [37]. Therefore, we reduced the number of model parameters by considering only the 12 temperatures (out of 44) at 38 m of height as outputs of the model. The speeds of the six dosers, which were proportional to their loads, represented the inputs into the model. The adopted structure of the model was as follows:

$$T_i(k) = -\sum_{n=1}^{N} a_{in} T_n(k-1) + \sum_{m=1}^{M} b_{im} d_m(k-1) + \zeta(k) \quad (2)$$

where T_i and d_m represent model output temperatures and input doser speeds, $N = 12$ and $M = 6$ are the numbers of outputs and inputs of the model, respectively, $i = (1, N)$ denotes the index of the output temperature, $\zeta(k)$ is the process noise, and a_{in} and b_{im} are the unknown model parameters. Equation (2) can be shown in a linear regression form

$$T_i(k) = W^T(k) X_i(k) + \zeta(k) \quad (3)$$

where $W^T(k) = [-T_1(k-1) \ldots - T_N(k-1) \;\; d_1(k-1) \ldots d_M(k-1)]$ is the regression vector of the model and $X_i^T(k) = [a_{i1} \ldots a_{iN} \;\; b_{i1} \ldots b_{iM}]$ is the parameter vector. Note that in the general case, the parameters are not constant and that the time index is omitted due to notation simplicity. We propose a parameter estimation approach based on a WRLS algorithm

$$J_\rho(k) = \sum_{i=0}^{k} \rho^{k-i} e^2(i) \quad (4)$$

where $e(k) = d(k) - W^T(k-1)X(k)$ is the prediction error and $\rho \in (0, 1]$ is the forgetting factor. Minimization of criterion (4) leads to a recursive identification procedure

$$\hat{W}(k) = \hat{W}(k-1) + K(k) e(k) \quad (5)$$

where $P(k)$ and $K(k)$ are given as

$$P(k) = \frac{1}{\rho}[P(k-1) - K(k) X^T(k) P(k-1)] \quad (6)$$

$$K(k) = P(k-1) X(k) [\rho + X(k) P(k-1) X(k)]^{-1}. \quad (7)$$

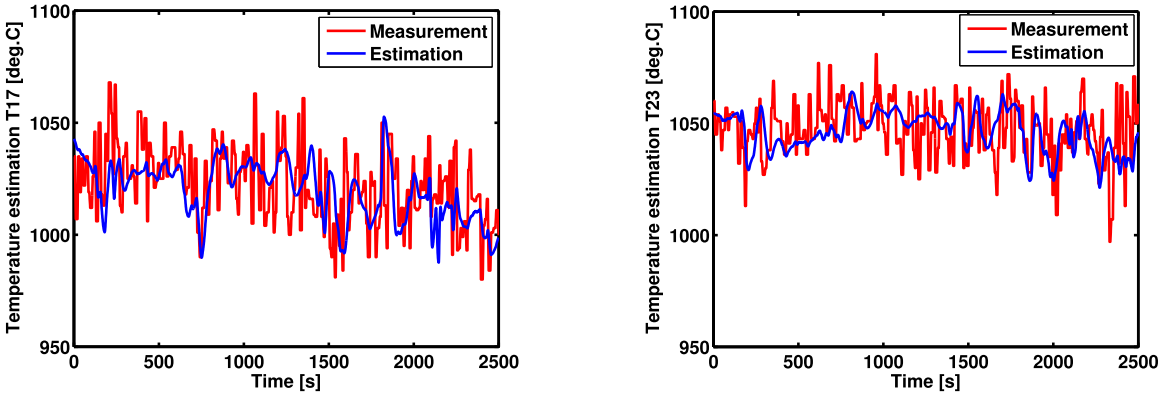

Fig. 7. Parameter estimation results: temperature measurements (red curve) and temperature estimations (blue curve) for T17 (left) and T23 (right).

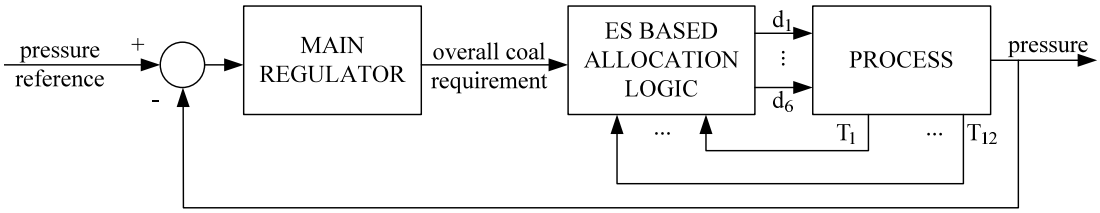

Fig. 8. Control algorithm structure.

In nonstationary conditions such as these, it is convenient to use $\rho < 1$, which assigns smaller weights to the former measurements. The application of this recursive procedure and its comparison to other adaptive variable forgetting factor algorithms is provided in detail in [38]. Our main motivation behind WRLS implementation was its robustness to the nonstationarities present in the combustion process. They are usually caused by the variable coal structure and properties. On the other hand, mill performance deteriorates with time due to their physical state, or significantly improves after an overhaul. Model verification was performed on real measurements obtained in the Nikola Tesla power plant, Serbia. Fig. 7 shows real temperatures at two representative sensors (red curve), compared with corresponding estimated model output temperatures (blue curve). As illustrated, the model managed to capture the system dynamics. Although the model was simplified, a thorough analysis of all model output temperatures showed that the WRLS identification procedure was satisfactory and encouraged the use of the model for simulations pertaining to control algorithm analysis.

IV. Coal Allocation Algorithm for Temperature Distribution Regulation

Fig. 8 shows the proposed control algorithm structure. The main regulator outputs the overall coal requirement based on the turbine pressure reference and measurement difference. This information is passed on to the distribution control block, which we introduce in this paper. The proposed approach to combustion distribution control relies on the formulation of a cost function to be optimized [39]. As noted earlier, process behavior is essentially dictated by the pair of opposite mills, rather than each mill separately. This enables a simpler structure of the control algorithm, since there are three instead of six control algorithm outputs. Let us introduce some assumptions prior to the control algorithm setup: 1) the overall coal requirement is determined by the outer control algorithm and is assumed to be known from the ESC perspective; 2) the dynamics of the proposed distribution algorithm should be slower than the dynamics of the main regulator whose sample time is $T = 200$ ms; and 3) the contribution of each feeder pair is the same and it is set to 1/3 of the overall coal demand. With this premise, the control task is reduced to determining the optimal coal allocation within each pair. Let us denote by n_1, n_2, and n_3 the ratio of d_1 to d_4, d_2 to d_5, and d_3 to d_6, respectively (corresponding to M61–M66 in Fig. 1). The main characteristic of tangentially fired boilers is the existence of a fireball in the center of the furnace, with the temperature being at its maximum at the focal point of the fireball. The temperature decreases with the distance from the central vortex toward the boiler walls. In other words, if all the conditions are uniform, the round flame core causes the same temperature at the same distance from the focus. However, a change in furnace and mill conditions leads to a flame shift toward the walls and an increase in temperature at corresponding pyrometers. Therefore, the goal to centralize the flame geometry leads to the cost function

$$J_n = \sum_{i=17}^{22} (T_i - T_{i+k})^2 \tag{8}$$

where parameter $k = 6$ provides the summation of diametrically opposite temperature differences and T_i is according to the notation of Fig. 3. Minimization of this cost function leads

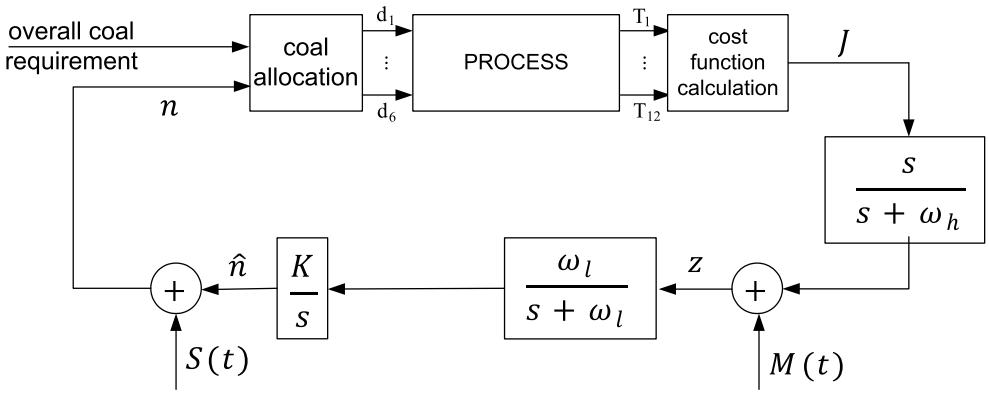

Fig. 9. Gradient-based ES algorithm for a dynamic multivariable nonlinear map.

to an elliptical flame configuration. In a perfect scenario, all three ratios are equal to one, meaning uniform coal distribution to six mills. That would result in a minimum value of the optimization function (around zero). This is rarely the case in practice, since there are many parameters that influence combustion: coal burning process, current condition of the mills, and so on. For practical reasons, the contribution of each mill is limited to [0.8, 1.2] of the overall dictated amount of coal. This bounds the ratio within each pair of mills to $n_i \in [2/3, 3/2], i = 1, 2, 3$. The constraints can be included in the optimization criterion resulting in

$$J = J_n + J_c$$
$$J_c = \sum_{i=1}^{3} C \left[\max \left(\frac{n_i - n_{\max}}{n_{\max}}, 0, \frac{n_{\min} - n_i}{n_{\min}} \right) \right]^2 \quad (9)$$

where $n_{\min} = 0.67$, $n_{\max} = 1.5$, and parameter $C = 5 \cdot 10^5$ is selected so as to insure the significance of the constraints in the overall criterion. The correction factor is equal to zero when n_i is within the preset bounds and increases for n_i out of this range. Since both J_n and J_c are formulated to be convex with zero minimum value, the overall optimization criterion is a convex function. Finally, the optimization problem reduces to the minimization of criterion (9) with respect to n_1, n_2, and n_3.

A. Extremum-Seeking Control

Once we have defined the cost function to be optimized, we propose the deployment of the ES algorithm using the perturbation signals in resolving the optimization problem. Fig. 9 shows the basic ES structure for the dynamic multivariable nonlinear map applied to the described combustion distribution control setup. It is important to emphasize that the perturbation frequencies should ensure a sufficient time-scale separation between the ES loop and the plant. For an input vector consisting of three variables $n = [n_1 \quad n_2 \quad n_3]^T$, perturbation signal $S(t)$ and demodulation signal $M(t)$ are of the following form:

$$S(t) = [a_1 \sin(\omega_1 t) \quad a_2 \sin(\omega_2 t) \quad a_3 \sin(\omega_3 t)] \quad (10)$$
$$M(t) = \left[\frac{1}{a_1} \sin(\omega_1 t) \quad \frac{1}{a_2} \sin(\omega_2 t) \quad \frac{1}{a_3} \sin(\omega_3 t) \right] \quad (11)$$

where perturbation frequencies should satisfy two conditions: 1) each two should be different ($\omega_i \neq \omega_j$) and 2) the ratio of each two should be rational ($\omega_i/\omega_j \in \mathbb{Q}$), $i, j = 1, 2, 3$, $i \neq j$.

The perturbation amplitude a and the diagonal matrix K with negative elements represent small parameters, which are responsible for stability and determine the convergence speed of the algorithm. There are several papers dealing with the analysis of stability and convergence of ES control for nonlinear dynamic systems [40], [41]. The role of the two filters is to decrease the effects of the perturbation signals, or, in other words, to eliminate the dc component of the optimized signal J (high-pass filter) and isolate a dc component of the product signal z necessary for gradient estimation (low-pass filter). Thus, the filters should have a slower time scale than the periodic perturbations and, therefore, the plant itself. If all the conditions are met, the algorithm converges, minimizing the cost function (9) obtained using the optimal value of input vector n^*.

V. Experimental Results

To verify the proposed ES control approach, we employed the model of the system, as described in Section III. The simulations were conducted on the time-varying parameters obtained from the WRLS algorithm. As stated earlier, the goal of our control algorithm is to regulate the position and the geometry of the flame inside the furnace, by minimizing the preset criterion (9). The real system includes processes with different dynamics. The main regulator operates with a sample time of $T = 200$ ms, because of rapid pressure changes. However, temperatures evolve slowly over time, so pyrometer data are acquired with a sample time of $T = 1$ s. Therefore, our control algorithm should operate with the same sample time, so the simulations were performed with the same sample time of 1 s. We introduce the reference speed to the algorithm, which represents the overall needed doser speed and is proportional to the overall coal requirement. Normally, this information is provided by the external control loop in charge of maintaining the desired fresh steam pressure. The dictated overall doser speed is shown in Fig. 10. As a first step of the algorithm, the reference speed is divided equally among

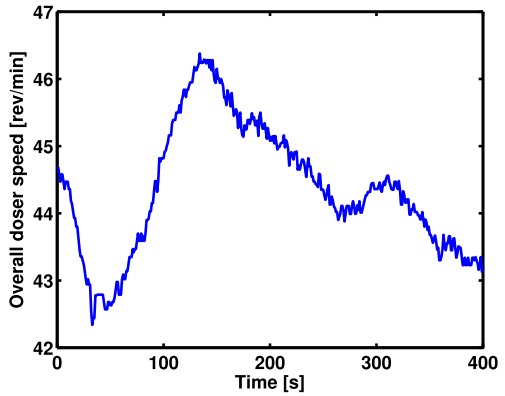

Fig. 10. Overall doser speed proportional to the overall coal load requirements.

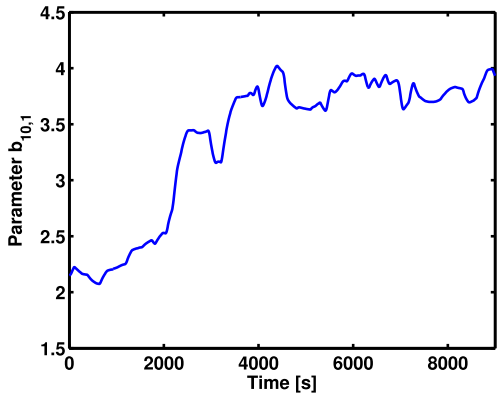

Fig. 11. Evolution of WRLS algorithm parameter during the active power reference change.

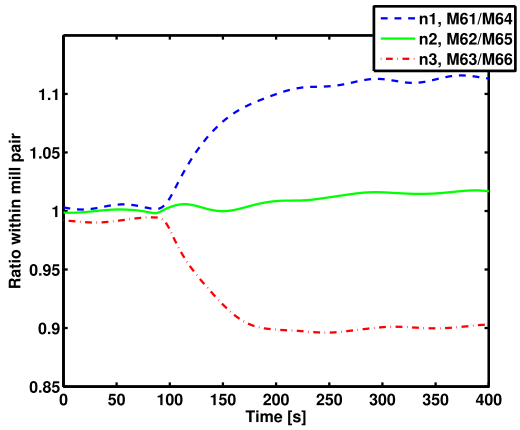

Fig. 12. Control signals: ratios within each mill pair.

three pairs of dosers. The objective of the ESC structure is to estimate the optimal ratios within these pairs.

One of the main conditions for proper implementation of the ES controller on a time-varying system is the time-scale separation between the system dynamics, ES controller, and plant changes. Namely, the ES controller should be slower than the slowest model mode and faster than the rate at which the model changes. The largest time constant of the modeled plant dynamics is around 40 s. On the other hand, the temperature process in the furnace is highly nonstationary, not only because of disturbances but also because of the changing demands manifested through the active power, steam flow, and pressure references. In order to illustrate these phenomena, we analyze the behavior of the system during the increase in the active block power from 0 to 350 MW, which corresponds to the biggest change in the system parameters. The usual gradient of power is from 2 to 5 MW/min. Fig. 11 shows WRLS algorithm parameter during this phase as it follows the changes successfully. Time constant that corresponds to the described process is around 500 s. Therefore, perturbation signals should have a slower time scale than 40 s and faster than 500 s. The adopted perturbation frequencies are 0.08, 0.06, and 0.05 rad/s. Parameters $a_1 = a_2 = a_3 = 0.002$ and a diagonal gain matrix $K = -\text{diag}(5 \cdot 10^{-10}, 5 \cdot 10^{-10}, 5 \cdot 10^{-10})$ were carefully chosen. These parameters were determined empirically. Imposing the constraints on the control signal would normally limit the selection of the appropriate parameter, and therefore the speed of the algorithm, in order to stay within the desired bounds. Introduction of these constraints through the penalty function gives us more freedom in that sense. The filter cutoff frequencies $\omega_l = [0.04, 0.04, 0.04]$ rad/s and $\omega_h = 0.04$ rad/s. The parameters were chosen to satisfy the qualitative convergence requirements explained in Section IV. However, the ESC convergence proof assumes a certain ODE model structure, which the combustion system, whose first-principles model includes many coupled nonlinear partial differential equations in 3-D, does not verify. Fig. 12 shows that in the beginning, all three ratios are close to one, meaning that all the mills contribute roughly the same to the control process. A disturbance was introduced into the model in terms of a pulse change in input model parameters, at time $t = 90$ s. After a transition period of around 100 s, control signals settle in a new steady state. The coal distribution within the second pair of mills stays almost unchanged, while the distribution in the other two pairs changes, to try and minimize the preset criterion. Signals include the sinusoidal perturbations, which correspond to the chosen frequencies. As a result, the control algorithm dictates mill M61 to provide around 55% and mill M64 around 45% of the coal required from that pair. Mills M63 and M65 encounter a similar scenario. Experience indicates that the flame geometry is influenced by the ratio of the doser speeds, rather than the speeds themselves, which was confirmed in these experiments. In other words, as long as the speed ratio in a particular direction was maintained, the flame center in that direction did not shift. Of course, one should bear in mind that a higher speed results in mill overload as a side effect, so there are limitations to the range within which the speed can be varied. This relative insensitivity of the flame geometry on the doser speeds was what enabled the employment of the ES algorithm, which is, otherwise, inapplicable to rapidly changing plant parameters. However, in this case, ES algorithm manages to adapt and slide the control parameters toward new values, which result in the minimization of the objective function.

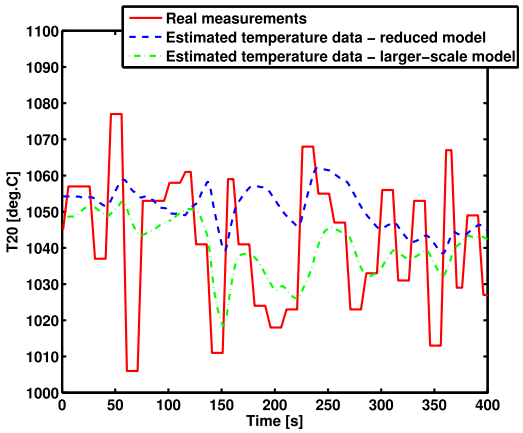

Fig. 13. Comparison of two WRLS models. Detail from the temperature T_{20} estimations.

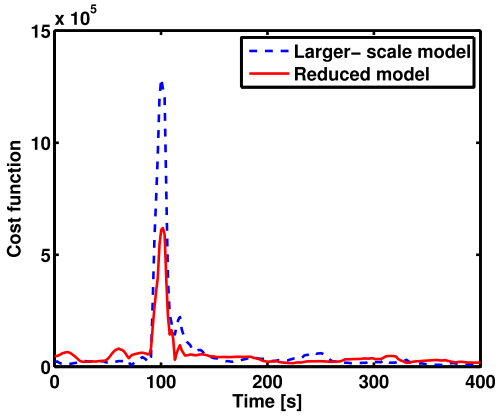

Fig. 14. Evolution of cost function upon the introduction of disturbance.

In order to additionally analyze the proposed control algorithm, we conducted testing on a significantly complex model expanded in both the spatial (including temperatures from the lower and upper levels) and temporal domain, namely, a third-order model with 36 temperatures as outputs and six doser speeds as inputs

$$T_i(k) = -\sum_{n=-12}^{N+12} a_{in} T_n(k-1) + a_{in+36} T_n(k-2) + a_{in+72} \times T_n(k-3) + \sum_{m=1}^{M} b_{im} d_m(k-1) + \zeta(k) \quad (12)$$

where indexes $n = -12$ to -1 correspond to the temperatures at the lower level at 23 m, and $n = 13$–24 correspond to the higher level at 43 m. Fig. 13 shows a representative medium-level temperature measurement (T_{20}) obtained from the real system, along with the corresponding temperature estimations of the reduced and complex models. Although the larger-scale model captures real process dynamics better, the differences between the two are not significant and they are below 2% of measured value. However, Fig. 13 shows significant differences between estimated and measured temperatures in some places. The main reasons for this are: 1) many disturbances in the furnace that cause sudden changes in temperature measurements (e.g., inhomogeneities of the aero-mixture and local explosions); 2) pyrometer measurements are contaminated by the constant noise inherent in the measurement method (e.g., particles of dust on the optical path); and 3) sample time of pyrometer measurements is 5 s. Therefore, the real measurements are expected to deviate from the model outputs. Additional improvements of the identification procedure are possible by tuning the algorithm parameters, e.g., a variable forgetting factor could lead to better temperature tracking. The forgetting factor was chosen as a tradeoff between robustness to disturbances and measurement noise and better convergence speed.

Further analysis of the controller originally designed on the reduced model included testing on the complex model. Fig. 14 shows a comparison of cost functions in these two cases. The plot shows a slight performance degradation when the controller was tested on the large-scale model. These results indicate that model (2) is sufficiently precise in describing the process dynamics and that the implementation of the designed controller on a real system should not encounter substantial performance degradation. To corroborate the fidelity of the presented models, we developed a large-scale model, which employs a finite-element method (FEM) for boiler geometry analysis and simulates several physical and chemical processes that are crucial for realistic temperature distribution calculations in the case of pulverized-coal combustion [42]–[44]. A detailed description of the mathematical model is provided in the Appendix. The simulations were executed using COMSOL Multiphysics software. Fig. 15 shows that temperature estimation by the FEM model includes dynamics, which is obviously neglected in WRLS models. However, careful analysis leads to the conclusion that deviation up to 15 °C between the models still makes the simplified WRLS model rather useful for this particular application. This is especially emphasized by the fact that the proposed control algorithm does not require a quality model.

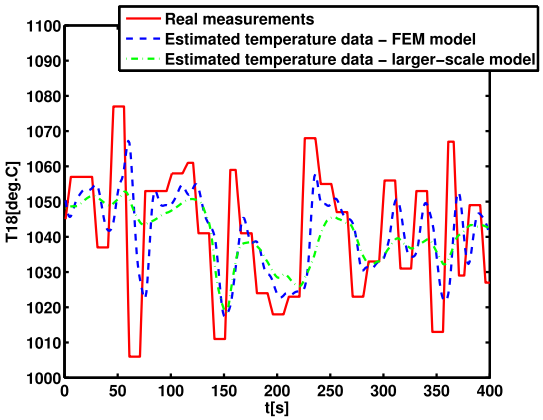

Fig. 15. Comparison of complex WRLS and FEM model. Detail from the temperature T_{20} estimations.

Fig. 16 shows a 2-D temperature distribution reconstruction based on the finite number of measurements. It illustrates

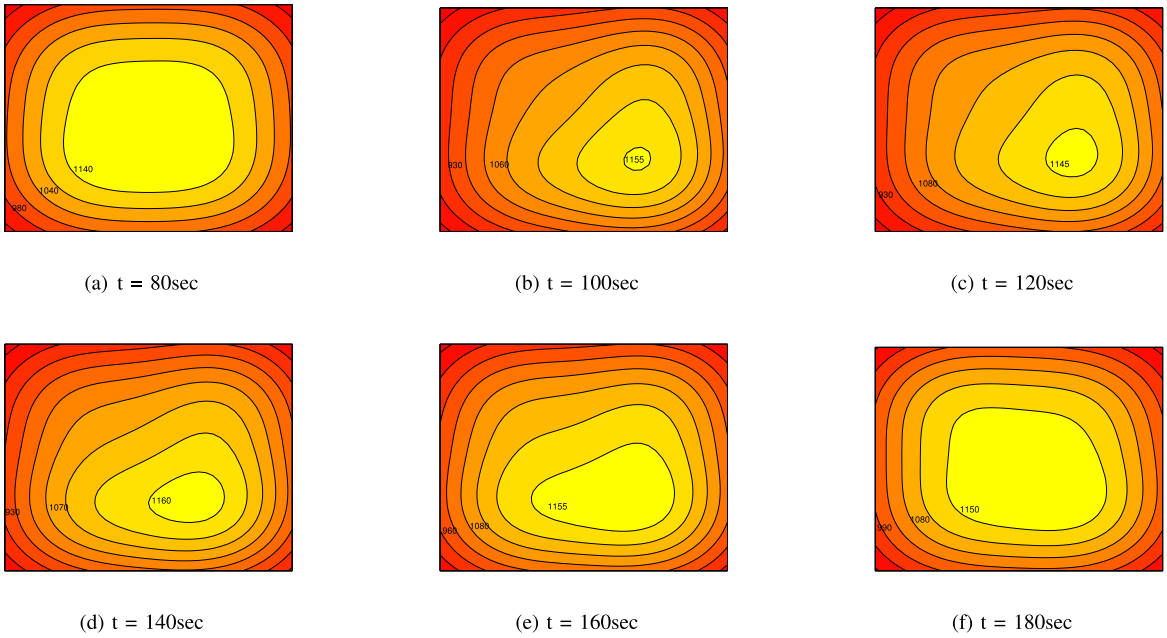

(a) t = 80sec (b) t = 100sec (c) t = 120sec

(d) t = 140sec (e) t = 160sec (f) t = 180sec

Fig. 16. Evolution of 2-D temperature distribution as a result of pulse disturbance at $t = 90$ s. Bright colors correspond to higher temperatures. Isotherms are given in °C. (a) $t = 80$ s. (b) $t = 100$ s. (c) $t = 120$ s. (d) $t = 140$ s. (e) $t = 160$ s. (f) $t = 180$ s.

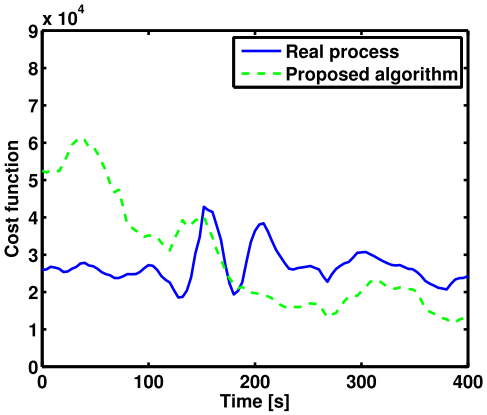

Fig. 17. Comparison of cost functions calculated using data obtained from the real process and in the simulation of the proposed algorithms.

flame behavior over a period of 100 s after a disturbance in model parameters. It is apparent that after the disturbance at $t = 90$ s, the flame slowly started to shift toward the front-right corner of the furnace. The peak in the cost function corresponds to the flame position closest to the corner of the furnace, at around $t = 100$ s. As the ES algorithm managed to readjust the control signals, the flame slowly moved back toward the center of the furnace. After this transient, the controller determined new optimal steady-state control parameters, which provide the central position of flame.

One of the initial assumptions we made was that each mill pair contributed equally to the firing process. Therefore, the comparison of the obtained results to the real measurement from the process would not be an objective indicator. In order to compare these two, let us employ the information about the real commanded doser speeds over mill pairs, generated by the operator in a real-case scenario. Based on the extensive experience that the operators have, they usually keep some of the mills in the manual operating mode at a preset value, while the other mills compensate the overall coal demand. Fig. 17 shows the cost function (9) in both cases. The measurement noise is not incorporated in the objective function derived from the ESC approach; however, it would not make a significant difference in this analysis. The proposed algorithm yields comparably good results in terms of reallocation within mill pairs, thus keeping the temperature inside the desired range.

VI. Conclusion

This paper considers an optimization algorithm of the thermal power plant combustion distribution process using the proposed ES algorithm. Prior to formulating a control law, the combustion process is extensively analyzed to provide insight into how spatial temperature distribution depends on the firing and coal dissipation over the mill circles. Cross-correlation analysis shows that the flame shift can be dictated by a pair of opposite mills. These conclusions helped understand the nature of the process and obtain an adequate combustion model for further simulations. Finally, this paper provides a possible solution for flame geometry regulation in the form of an optimal control problem with an objective function, which includes a set of constraints regarding control signals. Finally, we introduced the proposed control algorithm to the model of the combustion process. As a consequence of disturbances taking place inside the furnace, the flame was shifted toward the front of the furnace. The results show a transition of control signals to a new steady state, in a timely manner, providing an ellipsoid flame configuration. In addition, the introduction of constraints

into our objective function enables aggressive ES parameters and, hence, exhibits better convergence properties. In the real-case scenario, the reallocation of the coal depends on a broad experience of the operator. When compared with the real data obtained from the thermal power plant Nikola Tesla A, the algorithm performed very well. The proposed algorithm can be easily implemented and is reasonably fast, which is a necessity for a real-time online application.

APPENDIX

This section provides details of the development of a large-scale model based on the FEM. In preliminary simulations, we assume a somewhat simpler unit geometry and we model the boiler as a rectangular parallelepiped, with rectangular ducts (standing for the pulverized-coal aero-mixture) and secondary air inlets, as well as a recirculation air outlet. For these boundaries, we set appropriate boundary conditions that define fuel and air velocities, temperatures, and inflow mass fractions of the species that contribute to the fuel and the coflow air. The outlet is set with an outflow boundary condition, which suppresses excess air backflow. Conditions near the walls are described by "wall functions."

At this point, the physics of combustion inside the boiler is modeled to comprise multicomponent gaseous phase fluid flow with species mass transport, combustion, and heat transfer. The mass balances that describe transport and the reactions are given by diffusion-convection equations at steady state

$$\nabla \cdot (-D_i \nabla c_i) + \vec{u} \nabla c_i = R_i \tag{A.1}$$

where D_i and c_i stand for the diffusion coefficient and concentration of the species i, respectively, $\vec{u}$ is the velocity vector, and R_i is the species i production rate ($\mathrm{kg/m^3 s}$). When a turbulence model is used in a COMSOL Reacting Flow interface, the production rate of species i resulting from reaction j is modeled via the eddy-dissipation-model rate $r_{\mathrm{ED},j}$

$$R_{ij} = \upsilon_{ij} M_i r_{\mathrm{ED},j}. \tag{A.2}$$

Here, υ stands for the stoichiometric coefficient and M_i represents the molar mass of species i. The reaction rate r_{ED} defined by the eddy-dissipation model is given by [42]

$$r_{\mathrm{ED},j} = \frac{\alpha_j}{\tau} \rho \min \left[\min \left(\frac{\omega_r}{\upsilon_{rj} M_r} \right), \beta \sum_p \left(\frac{\omega_p}{\upsilon_{pj} M_p} \right) \right] \tag{A.3}$$

where τ is the mixing time scale of the turbulence, ρ is the mixture density, ω is the species mass fraction, and the parameter β models the activation energy [42]. The properties of reactants are indicated using a subscript r while product properties are denoted by the subscript p.

In the combustion process, we assume three exothermic reactions, char combustion $\mathrm{C} + \mathrm{O_2} \rightarrow \mathrm{CO_2}$, and volatiles reactions

$$\mathrm{CO} + 0.5\mathrm{O_2} \rightarrow \mathrm{CO_2} \tag{A.4}$$

$$\mathrm{H_2} + 0.5\mathrm{O_2} \rightarrow \mathrm{H_2O}. \tag{A.5}$$

In order to simplify the model to some extent, the molecular reaction rate of the reactions is assumed to be infinitely fast. This is achieved by prescribing unrealistically high rate constants for the reactions.

The heat of the reactions (i.e., the change in enthalpy following each reaction) is defined from the heat formed by the products and reactants:

$$\triangle H_{\mathrm{reaction}} = \sum_{\mathrm{products}} \triangle H_f - \sum_{\mathrm{reactants}} \triangle H_f. \tag{A.6}$$

The heat of formation $\triangle H_f$ for each species is taken from [43]. The heat release is included in the model by adding a Heat Source feature to the COMSOL Heat Transfer in Fluids user interface. The applied heat source ($\mathrm{W/m^3}$) is defined as

$$q = \sum_k r_{\mathrm{ED},k} \triangle H_{f,k} \tag{A.7}$$

where index $k = \{1, 2, 3\}$ sums up the three assumed chemical reactions.

For an accurate prediction of the temperature distribution, it is important to account for temperature dependence of the heat capacities of the species. In the current model, interpolation functions for the heat capacity at constant pressure for each of the species are defined using the values at three different temperatures given in [43]. The heat capacity of the mixture $c_{p,\mathrm{mix}}$ is computed as a mass fraction weighted mean of the individual heat capacities

$$c_{p,\mathrm{mix}} = \sum_i \frac{\omega_i C_{p,i}}{M_i}. \tag{A.8}$$

Finally, the heat transfer is modeled using

$$\rho c_{p,\mathrm{mix}} \overrightarrow{u} \cdot \nabla T = \nabla \cdot (k_{\mathrm{eq}} \nabla T) + q \tag{A.9}$$

with k_{eq} standing for the equivalent thermal conductivity of the solid particles/fluid mixture, computed as a mass fraction weighted sum of the individual thermal conductivities. In addition, thermal conductivity is assumed to be temperature dependent, according to COMSOL Material Library data.

ACKNOWLEDGMENT

The authors would like to thank their colleague Marko Krstić for his help concerning the finite-element method model derivation and implementation in COMSOL Material Library. In addition, they would also like to thank the support from the Ministry of Education and Science of the Republic of Serbia, research projects TR32038 and III42007.

REFERENCES

[1] C. Yin, S. Caillat, J.-L. Harion, B. Baudoin, and E. Perez, "Investigation of the flow, combustion, heat-transfer and emissions from a 609 MW utility tangentially fired pulverized-coal boiler," *Fuel*, vol. 81, no. 8, pp. 997–1006, 2002.

[2] D. Flynn, *Thermal Power Plant Simulation and Control*. London, U.K.: The Institution of Engineering and Technology, 2003.

[3] M. Stöllinger, B. Naud, D. Roekaerts, N. Beishuizen, and S. Heinz, "PDF modeling and simulations of pulverized coal combustion—Part 1: Theory and modeling," *Combustion Flame*, vol. 160, no. 2, pp. 384–395, 2013.

[4] M. Stöllinger, B. Naud, D. Roekaerts, N. Beishuizen, and S. Heinz, "Pdf modeling and simulations of pulverized coal combustion—Part 2: Application," *Combustion Flame*, vol. 160, no. 2, pp. 396–410, 2013.

[5] D. French, *Metallurgical Failures in Fossil Fired Boilers*. Hoboken, NJ, USA: Wiley, 1993.

[6] C. F. M. Coimbra, J. L. T. Azevedo, and M. G. Carvalho, "3-D numerical model for predicting NO_x emissions from an industrial pulverized coal combustor," *Fuel*, vol. 73, no. 7, pp. 1128–1134, 1994.
[7] R. Saripalli, T. Wang, and B. Day, "Simulation of combustion and thermal flow in an industrial boiler," in *Proc. 27th Ind. Energy Technol. Conf.*, New Orleans, LA, USA, 2005, pp. 1–15.
[8] T. Asotani, T. Yamashita, H. Tominaga, Y. Uesugi, Y. Itaya, and S. Mori, "Prediction of ignition behavior in a tangentially fired pulverized coal boiler using CFD," *Fuel*, vol. 87, no. 4, pp. 482–490, 2008.
[9] E. Korytnyi, R. Saveliev, M. Perelman, B. Chudnovsky, and E. Bar-Ziv, "Computational fluid dynamic simulations of coal-fired utility boilers: An engineering tool," *Fuel*, vol. 88, no. 1, pp. 9–18, 2009.
[10] H.-C. Zhou *et al.*, "Experimental investigations on visualization of three-dimensional temperature distributions in a large-scale pulverized-coal-fired boiler furnace," *Proc. Combustion Inst.*, vol. 30, no. 1, pp. 1699–1706, 2005.
[11] H. B. Vuthaluru and R. Vuthaluru, "Control of ash related problems in a large scale tangentially fired boiler using CFD modelling," *Appl. Energy*, vol. 87, no. 4, pp. 1418–1426, 2010.
[12] Z. Hao, X. Qian, K. Cen, and F. Jianren, "Optimizing pulverized coal combustion performance based on ANN and GA," *Fuel Process. Technol.*, vol. 85, nos. 2–3, pp. 113–124, 2004.
[13] F. Si *et al.*, "Optimization of coal-fired boiler scrs based on modified support vector machine models and genetic algorithms," *Fuel*, vol. 88, no. 5, pp. 806–816, 2009.
[14] M. Bhowmick and S. C. Bera, "An approach to optimum combustion control using parallel type and cross-limiting type technique," *J. Process Control*, vol. 22, no. 1, pp. 330–337, 2012.
[15] X.-F. Wang and H.-C. Zhou, "Simulation on an optimal combustion control strategy for 3-D temperature distributions in tangentially pc-fired utility boiler furnaces," *J. Environ. Sci.*, vol. 17, no. 2, pp. 305–308, 2005.
[16] X. Sun, H. Yue, and H. Wang, "Modelling and control of the flame temperature distribution using probability density function shaping," *Trans. Inst. Meas. Control*, vol. 28, no. 5, pp. 401–428, 2006.
[17] M. Krstić, "Performance improvement and limitations in extremum seeking control," *Syst. Control Lett.*, vol. 39, no. 5, pp. 313–326, 2000.
[18] D. Nešić, "Extremum seeking control: Convergence analysis," *Eur. J. Control*, vol. 15, no. 3, pp. 331–347, 2009.
[19] M. Guay, "A time-varying extremum-seeking control approach for discrete-time systems," *J. Process Control*, vol. 24, no. 3, pp. 98–112, 2014.
[20] H.-H. Wang, S. Yeung, and M. Krstić, "Experimental application of extremum seeking on an axial-flow compressor," *IEEE Trans. Control Syst. Technol.*, vol. 8, no. 2, pp. 300–309, Mar. 2000.
[21] M. Guay, D. Dochain, and M. Perrier, "Adaptive extremum seeking control of continuous stirred tank bioreactors with unknown growth kinetics," *Automatica*, vol. 40, no. 5, pp. 881–888, 2004.
[22] C. Yin, B. Stark, Y. Chen, and S.-M. Zhong, "Adaptive minimum energy cognitive lighting control: Integer order vs fractional order strategies in sliding mode based extremum seeking," *Mechatronics*, vol. 23, no. 7, pp. 863–872, 2013.
[23] A. Ghaffari, M. Krstic, and S. Seshagiri, "Power optimization and control in wind energy conversion systems using extremum seeking," in *Proc. IEEE Amer. Control Conf. (ACC)*, Jun. 2013, pp. 2241–2246.
[24] Y. A. Chang and S. J. Moura, "Air flow control in fuel cell systems: An extremum seeking approach," in *Proc. Amer. Control Conf. (ACC)*, Jun. 2009, pp. 1052–1059.
[25] M. Guay and T. Zhang, "Adaptive extremum seeking control of nonlinear dynamic systems with parametric uncertainties," *Automatica*, vol. 39, no. 7, pp. 1283–1293, 2003.
[26] N. J. Killingsworth, S. M. Aceves, D. L. Flowers, and M. Krstic, "Extremum seeking tuning of an experimental HCCI engine combustion timing controller," in *Proc. Amer. Control Conf. (ACC)*, Jul. 2007, pp. 3665–3670.
[27] C. Zhang and R. Ordonez, "Numerical optimization-based extremum seeking control with application to ABS design," *IEEE Trans. Autom. Control*, vol. 52, no. 3, pp. 454–467, Mar. 2007.
[28] W. Nwesaty, A. I. Bratcu, and A. Hably, "Extremum seeking control techniques applied to photovoltaic systems with multimodal power curves," in *Proc. Int. Conf. Renewable Energy Res. Appl. (ICRERA)*, Oct. 2013, pp. 85–90.
[29] E. Schuster, C. Romero, Z. Yao, and F. Si, "Integrated real-time optimization of boiler and post-combustion system in coal-based power plants via extremum seeking," in *Proc. IEEE Int. Conf. Control Appl. (CCA)*, Sep. 2010, pp. 2184–2189.
[30] M. S. Stanković, K. H. Johansson, and D. M. Stipanović, "Distributed seeking of nash equilibria with applications to mobile sensor networks," *IEEE Trans. Autom. Control*, vol. 57, no. 4, pp. 904–919, Apr. 2012.
[31] S. L. Brunton, X. Fu, and J. N. Kutz, "Extremum-seeking control of a mode-locked laser," *IEEE J. Quantum Electron.*, vol. 49, no. 10, pp. 852–861, Oct. 2013.
[32] B. G. B. Hunnekens, M. A. M. Haring, N. V. D. Wouw, and H. Nijmeijer, "Steady-state performance optimization for variable-gain motion control using extremum seeking," in *Proc. IEEE 51st Annu. Conf. Decision Control (CDC)*, Dec. 2012, pp. 3796–3801.
[33] C. Zhang and R. Ordonez, "Extremum seeking control based on numerical optimization and state regulation—Part II: Robust and adaptive control design," in *Proc. 45th IEEE Conf. Decision Control*, Dec. 2006, pp. 4460–4465.
[34] M. Haring, N. van de Wouw, and D. Nešić, "Extremum-seeking control for nonlinear systems with periodic steady-state outputs," *Automatica*, vol. 49, no. 6, pp. 1883–1891, 2013.
[35] H. Yu and Ü. Özgüne, "Adaptive tracking control via extremum-seeking method," *IFAC Proc. Vols.*, vol. 38, no. 1, pp. 259–264, 2005.
[36] M. Guay and D. J. Burns, "A comparison of extremum seeking algorithms applied to vapor compression system optimization," in *Proc. Amer. Control Conf. (ACC)*, Jun. 2014, pp. 1076–1081.
[37] G. Kvašcev, M. Jakovljević, V. Stevanović, and Ž. Đurović, "One approach to combustion control in thermal power plants," in *Proc. POWER-GEN Eur. Conf.*, 2013, pp. 1–14.
[38] A. Marjanović, S. Vujnović, V. Papic, and P. Todorov, "Robust parameter estimation of the thermal power plant combustion process," in *Proc. Int. Conf. Electr., Electron. Comput. Eng. (IcETRAN)*, 2014, pp. AUI1.1.1-5.
[39] A. Marjanović, M. Krstić, Z. Djurović, G. Kvascev, and V. Papic, "Combustion distribution control using the extremum seeking algorithm," *J. Phys. Conf. Ser.*, vol. 570, no. 5, p. 052001, 2014.
[40] M. Krstić and H.-H. Wang, "Stability of extremum seeking feedback for general nonlinear dynamic systems," *Automatica*, vol. 36, no. 4, pp. 595–601, 2000.
[41] Y. Tan, D. Nešić, and I. Mareels, "On non-local stability properties of extremum seeking control," *Automatica*, vol. 42, no. 6, pp. 889–903, 2006.
[42] B. Magnussen and B. Hjertager, "On mathematical modeling of turbulent combustion with special emphasis on soot formation and combustion," in *Proc. Symp. (Int.) Combustion*, 1977, vol. 16. no. 1, pp. 719–729.
[43] A. Frassoldati, T. Faravelli, and E. Ranzi, "The ignition, combustion and flame structure of carbon monoxide/hydrogen mixtures. Note 1: Detailed kinetic modeling of syngas combustion also in presence of nitrogen compounds," *Int. J. Hydrogen Energy*, vol. 32, no. 15, pp. 3471–3485, 2007.
[44] C. da Silva, M. L. Indrusiak, and A. Beskow, "CFD analysis of the pulverized coal combustion processes in a 160 MWe tangentially-fired-boiler of a thermal power plant," *J. Brazilian Soc. Mech. Sci. Eng.*, vol. 32, no. 4, pp. 427–436, 2010.

Aleksandra Marjanović received the Dipl.-Ing. and M.Sc. degrees from the Faculty of Electrical Engineering, University of Belgrade, Belgrade, Serbia, in 2009 and 2010, respectively, where she is currently pursuing the Ph.D. degree.

In 2009, she was an Intern with IHP, Leibniz-Institute for Innovative Microelectronics, Frankfurt, Germany. In 2013, she visited the University of California at San Diego, La Jolla, CA, USA. As a teaching assistant with the Signals and Systems Department, she is involved in several courses. She has authored/presented several papers in international scientific journals/conferences. Her current research interests include signal processing and estimation theory, system modeling and identification and their application in fault detection, and isolation techniques and implementation of optimal, fault tolerant control algorithms.

Ms. Marjanović was a recipient of the Best Paper Award at the Conference on Electrical, Electronic and Computing Engineering in 2011.

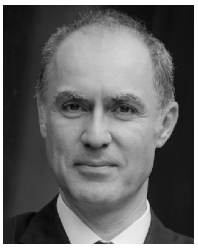

Miroslav Krstić (S'92–M'95–SM'99–F'02) received the bachelor's degree in electrical engineering from the University of Belgrade, Belgrade, Serbia, in 1989, and the Ph.D. degree from the University of California at Santa Barbara, Santa Barbara, CA, USA, in 1994.

He is the Founding Director of the Cymer Center for Control Systems and Dynamics, University of California at San Diego (UCSD), La Jolla, CA, USA. He also serves as an Associate Vice Chancellor for Research, UCSD. He has coauthored 11 books and 250 journal articles on adaptive, nonlinear, and stochastic control, extremum seeking, control of PDE systems including turbulent flows, and control of delay systems.

Dr. Krstić is a Fellow of the IFAC, the ASME, the SIAM, and the IET (U.K.), an Associate Fellow of the AIAA, and a Foreign Member of the Academy of Engineering Sciences of Serbia, Belgrade, Serbia. He holds the Alspach Endowed Chair.

Željko Đurović received the Dipl.-Ing., M.Sc. and Ph.D. degrees from the Faculty of Electrical Engineering, University of Belgrade, Belgrade, Serbia, in 1988, 1989 and 1994, respectively.

He was with the Research and Development Institute for Telecommunications, Belgrade, and the Radars Department from 1988 to 1989. Since 1989, he has been with the Faculty of Electrical Engineering, University of Belgrade, where he is currently a Full Professor. He held the post-doctoral fellow position with the Instituto Superior Technico, Lisbon, Portugal, in 2000. From 2000 to 2002 he was with Visteon GmbH, Cologne, Germany, as a Specialist for control strategies for CO2 refrigeration systems in the automotive industry. His areas of expertise include system control, digital signal processing, theory of estimation and stochastic systems, and pattern recognition. He currently teaches different undergraduate and postgraduate courses with the Department of Signals and Systems.

Branko Kovačević (M'93–SM'14) received the B.Sc., M.Sc., and Ph.D. degrees from the University of Belgrade, Belgrade, Serbia, in 1975, 1980, and 1984, respectively.

In 1981, he joined the Faculty of Electrical Engineering, University of Belgrade, where he is presently a Full Professor. He is the author of eight books and over 80 papers in scientific journals. His research interests lie in the fields of robust estimation, system identification, adaptive and nonlinear filtering, optimal and adaptive control, and digital signal processing.

Prof. Kovačević was a recipient of the Outstanding Research Prize of the Institute of Applied Mathematics and Electronics, the Prize of the Serbian Association for Informatics, the Prize of the Association of Radio Systems Engineers, and others. He is a member of the EURASIP, the WSAES, a member of a national association ETRAN, and a corresponding member of the Academy of Engineering Sciences of Serbia. He is also a Reviewer of the IEEE Transactions, IFAC *Automatica*, and *Signal Processing*.